Lett. **83**, 137 (1987).
3. J. Phipps Morgan, *Geophys. Res. Lett.* **14**, 1238 (1987).
4. D. W. Sparks and E. M. Parmentier, *Earth Planet Sci. Lett.* **105**, 368 (1991).
5. D. McKenzie, *J. Petrol.* **25**, 713 (1984); N. M. Ribe, *Geophys. J. R. Astron. Soc.* **83**, 487 (1985); M. J. Daines and F. M. Richter, *Geophys. Res. Lett.* **15**, 1459 (1988).
6. W. Su and W. R. Buck, *J. Geophys. Res.* **98**, 12191 (1993).
7. E. M. Parmentier and J. Phipps Morgan, *Nature* **348**, 325 (1990).
8. X. Wang, J. R. Cochran, G. A. Barth, *J. Geophys. Res.* **101**, 17927 (1996); G. A. Barth and J. C. Mutter, *ibid.*, p. 17951.
9. P. C. Hess, in *Mantle Flow and Melt Generation at Mid Ocean Ridges*, J. Phipps-Morgan, D. K. Blackman, J. Sinton, Eds. (American Geophysical Union, Washington, DC, 1992), pp. 67–102.
10. V. J. M. Salters and S. R. Hart, *Nature* **342**, 420 (1989); P. D. Beattie, *ibid.* **363**, 63 (1993); R. S. White, D. McKenzie, R. K. O'Nions, *J. Geophys. Res.* **97**, 19683 (1992).
11. P. J. Wyllie, *J. Geophys. Res.* **76**, 1328 (1971).
12. W. J. Su, R. L. Woodward, A. M. Dziewonski, *Nature* **360**, 149 (1992).
13. Fifty of the 51 OBSs were equipped with three-component, 1-Hz seismometers (model L4C, Mark Products) as well as either a hydrophone or Cox-Webb differential pressure gauge (DPG) to record pressure variations. One was equipped only with a hydrophone. Several methods for deploying, leveling, filtering, and recording were used by four instrument groups. Data were recorded at either 16 or 32 samples per second, except during the seismic refraction phase of the experiment when higher rates were used. Instrument response characteristics were derived for each type of instrument and tested by comparing corrected waveforms of earthquakes at adjacent stations. The OBSs operated independently on battery power, and no data were transmitted back to the recording ship. After correction for clock drift, the timing errors are estimated to be less than 0.01 s. After reaching the sea floor, each OBS was located precisely by acoustically ranging to a transponder from the ship, which was navigated with the P-code Global Positioning System. Locations are estimated to be accurate within about 10 m. At the end of the experiment, acoustic signals were sent to release the weights (anchors) of each OBS. Fifty of the 51 OBSs were recovered. To reduce noise, in three of the four basic OBS designs we deployed the seismometer package separately from the recording package after reaching the sea floor. This mechanical deployment procedure was the most serious instrumental problem in the experiment. The seismometer package did not deploy properly at 20 sites. Seismic records from these OBSs were limited to the waves with pressure components, including *P* waves, *S*-to-*P* converted phases, and Rayleigh surface waves.
14. D. S. Scheirer, D. W. Forsyth, M.-H. Cormier, K. C. Macdonald, *Science* **280**, 1221 (1998).
15. D. R. Toomey *et al.*, *ibid.*, p. 1224.
16. D. W. Forsyth, S. C. Webb, L. M. Dorman, Y. Shen, *ibid.*, p. 1235.
17. C. J. Wolfe and S. C. Solomon, *ibid.*, p. 1230.
18. S. C. Webb and D. W. Forsyth, *ibid.*, p. 1227.
19. M. K. McNutt and A. V. Judge, *ibid.* **248**, 969 (1990); J. Phipps Morgan, W. J. Morgan, Y.-S. Zhang, W. J. F. Smith, *J. Geophys. Res.* **100**, 12573 (1995).
20. U. H. Faul, D. R. Toomey, H. S. Waff, *Geophys. Res. Lett.* **21**, 29 (1994).
21. C. H. Langmuir, E. M. Klein, T. Plank, in (9), pp. 183–280.
22. Y. Shen, A. F. Sheehan, K. G. Dueker, C. de Groot-Hedlin, H. Gilbert, *Science* **280**, 1232 (1998).
23. S.-H. Hung and D. W. Forsyth, *Eos* **78**, F688 (1997).
24. S. Bazin *et al.*, *Geophys. Res. Lett.*, in press.
25. J. P. Canales, R. S. Detrick, S. Bazin, A. J. Harding, J. A. Orcutt, *Science* **280**, 1218 (1998).
26. J. J. Mahoney *et al.*, *Earth Planet. Sci. Lett.* **121**, 173 (1994).
27. M. Spiegelman and T. Elliott, *ibid.* **118**, 1 (1993).
28. M. Jull and D. McKenzie, *J. Geophys. Res.* **101**, 21815 (1996).
29. W. H. F. Smith and D. T. Sandwell, *ibid.* **99**, 21803 (1994).
30. The MELT Experiment is part of the RIDGE (Ridge Inter-Disciplinary Global Experiments) program and is funded by NSF.

18 February 1998; accepted 21 April 1998

Off-Axis Crustal Thickness Across and Along the East Pacific Rise Within the MELT Area

J. Pablo Canales,* Robert S. Detrick, Sara Bazin, Alistair J. Harding, John A. Orcutt

Wide-angle seismic data along the Mantle Electromagnetic and Tomography (MELT) arrays show that the thickness of 0.5- to 1.5-million-year-old crust of the Nazca Plate is not resolvably different from that of the Pacific Plate, despite an asymmetry in depth and gravity across this portion of the East Pacific Rise. Crustal thickness on similarly aged crust on the Nazca plate near a magmatically robust part of the East Pacific Rise at 17°15′S is slightly thinner (5.1 to 5.7 kilometers) than at the 15°55′S overlapping spreading center (5.8 to 6.3 kilometers). This small north-south off-axis crustal thickness difference may reflect along-axis temporal variations in magma supply, whereas the across-axis asymmetry in depth and gravity must be caused by density variations in the underlying mantle.

The MELT area between 15° to 19°S (*1*–*7*) shows a pronounced asymmetry across the East Pacific Rise (EPR) in several characteristics such as spreading rate (faster to the east) (*5*, *8*), subsidence rate (slower on the west) (*6*), and gravity anomaly [a less pronounced increase of the mantle Bouguer anomaly (MBA) away from the ridge axis on the Pacific Plate than on the Nazca Plate] (*7*). This asymmetry in MBA across the EPR in the MELT area can be interpreted in terms of variations in crustal thickness or in crustal or mantle density. The lower MBA and shallower seafloor on the Pacific Plate ~100 km west of the rise axis (*7*) could mean that the oceanic crust is ~1 km thicker than similarly aged crust east of the rise axis or that the mantle there is hotter and less dense (*9*). We used wide-angle seismic data collected as part of the MELT experiment to determine the crustal thickness variations across and along the EPR to evaluate the crustal contribution to the asymmetry in regional depth and gravity anomalies across the EPR in this area.

The data were recorded by 15 ocean-bottom seismometers (OBS) (*10*) deployed along three seismic refraction lines (Fig. 1). The northern line along the secondary MELT array was 360 km long and crossed the EPR a few kilometers north of the 15°55′S overlapping spreading center (OSC), and included five instruments (OBS sites 3, 4, 5, 7, and 8) spaced 40 to 90 km apart (hereafter referred to as line 1). Ten instruments were deployed along the primary MELT array, which intersects the rise axis near 17°15′S where a shallow and robust axial high is present (*7*). Four of these instruments (OBS sites 21, 23, 24, and 26), spaced 15 to 50 km apart, were located on the Nazca Plate along a line ~160 km in length (line 2). The remaining six instruments (OBS sites 39, 40, 42, 43, 45, and 46), spaced 15 to 80 km apart, were located on the Pacific Plate along a line ~230 km in length (line 3).

The seismic source for this experiment was a 4450-in^3 airgun array aboard the R/V *Melville* fired at a 100-s repetition rate. All of the OBS record sections showed clear crustal refractions (Pg arrivals) and Moho reflections (PmP arrivals); upper mantle refractions (Pn arrivals) were observed on some of the receivers (Table 1). The selected picks were analyzed by ray trace modeling (*11*). We determined the crustal velocity structure from Pg arrivals of diving waves turning up to ~3.0 to 3.5 km below the seafloor (Fig. 2). Despite some differences along each profile, the data showed that the top of the crust consists of a layer ~200 m thick in which the velocities increase from 2.5 to 4.0 km/s. These velocities are not directly constrained by turning rays in the uppermost crust, but this combination of velocity and thickness is required to match the delay of the Pg arrivals at the smallest shot-receiver ranges. Below this layer, crustal velocities increase from 4.0 to 7.0 km/s at a sub-seafloor depth of 3.0 to

J. P. Canales and R. S. Detrick, Department of Geology and Geophysics, Woods Hole Oceanographic Institution, 360 Woods Hole Road, Woods Hole, MA 02543, USA. S. Bazin, A. J. Harding, J. A. Orcutt, Institute of Geophysics and Planetary Physics, Scripps Institution of Oceanography, University of California San Diego, La Jolla, CA 92093–0225, USA.

*To whom correspondence should be addressed. E-mail: juan@sienna.whoi.edu

3.5 km (Fig. 3). Our interpretation of the upper and middle crustal velocity structure agrees with that reported by Bazin *et al.* (*12*), who used a tomographic inversion, along lines 2 and 3. We modeled the lowermost crust with a ~2.5-km-thick layer with P-wave velocities from 7.0 to 7.1 km/s on the Nazca Plate and up to 7.2 km/s on the Pacific Plate (*13*), although diving waves alone do not constrain lower crustal velocities below ~3.0 to 3.5 km.

We determined the crustal thickness along these lines by fitting the PmP and Pn arrivals for the upper crustal velocity structure obtained from the Pg arrivals and varying the thickness of the lower crust. We assumed that the Moho is a flat interface, and we modified its depth in 100-m steps to find the best fit to the PmP and Pn travel times (Fig. 4). We investigated several models in which the Moho dips toward and away from the ridge axis, but the results did not differ from a constant-depth Moho except along line 3, where a dipping Moho away from the ridge at a rate of 150 m every 100 km improved the fit.

Along line 1, PmP and Pn arrivals observed on receivers east of the ridge axis were fit with a crustal thickness of 5.8 to 6.3 km, whereas on the Pacific Plate, data were fit with a crustal thickness of 5.4 to 6.2 km (Fig. 4). The best fitting crustal thickness along line 2 is 5.1 to 5.7 km, and it is 4.8 to 5.6 km along line 3. These crustal thickness estimates are consistent with the two-way travel time to Moho of ~1.7 s observed on multichannel seismic reflection profiles in this area (*12*). There is a small (~0.6 km maximum) difference in crustal thickness between the northern and southern lines (Fig. 4). This difference is most apparent on the Nazca Plate; there is not a resolvable north-south difference in crustal thickness on the Pacific Plate. Upper crustal velocities at OBS site 26 on line 2 are also slightly lower than at OBS site 3 on line 1 (both sites are located on crust of comparable age) (Figs. 1 and 3). Thus, on average, the crust on the eastern flank of the EPR at 17°15′S is slightly thinner and has somewhat lower

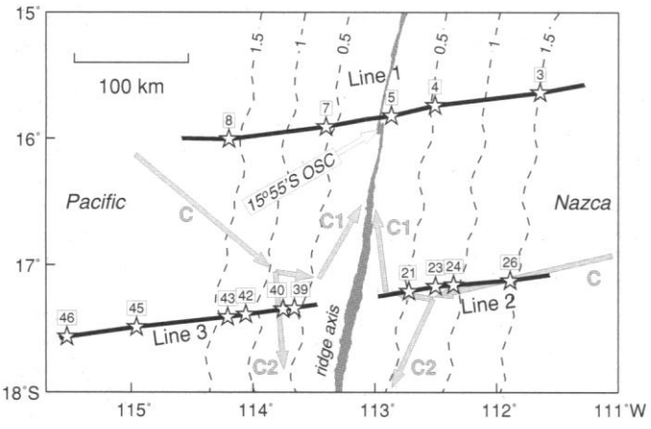

Fig. 1. Location map. Thick solid lines are seismic refraction profiles line 1, line 2, and line 3; stars show the location of the receivers used in this study, and the dark gray area indicates the location of the ridge axis (depths shallower than 2800 m). Dashed lines are isochrons labeled in mega-annum. Note that line 1 crosses the EPR a few kilometers north of the 15°55′S OSC (a deep and narrow section of the ridge), while lines 2 and 3 are located flankward of an inflated and shallow section of the ridge. Light gray arrows show the off-axis trace of three OSCs (C, C1, C2) that affected the study area (*5*). Crust along line 2 was generated under the influence of OSC C and the early development of OSC C1. On the western flank, only a small segment at location 40 was affected by OSC C2. Thus, along-axis crustal thickness variations are more likely to occur on the Nazca Plate than on the Pacific Plate.

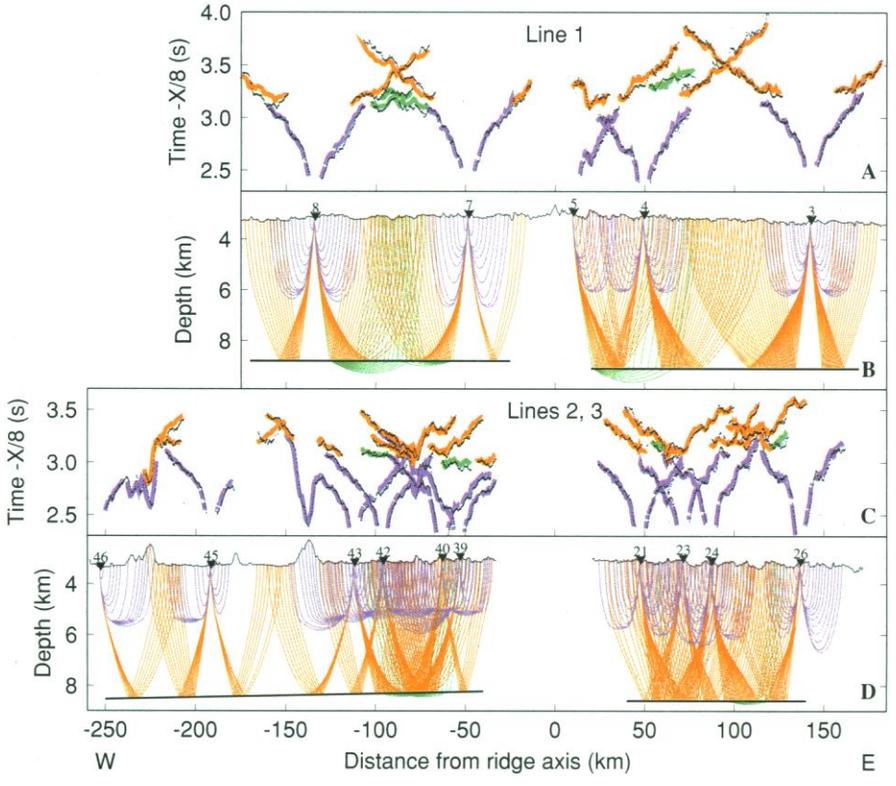

Fig. 2. (**A**) Observed (black dots) and predicted travel times (color bands: blue for Pg, orange for PmP, and green for Pn arrivals) at the receivers on line 1. Vertical scale shows the travel time corrected for a velocity reduction of 8 km/s. (**B**) Ray coverage (only 1 of every 10 rays is plotted) along line 1. Pg rays (turning rays within the crust) are shown in blue, PmP (reflected rays in the Moho) in orange, and Pn (rays turning below the Moho) in green. Triangles denote the position of the receivers, thin solid line is the seafloor topography, and thick solid line shows the Moho that best fits the data. (**C**) and (**D**) are the same as (A) and (B), respectively, for lines 2 and 3.

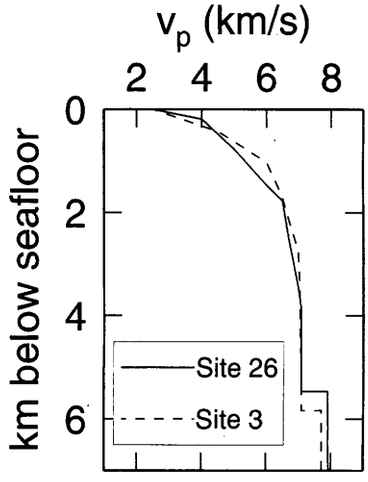

Fig. 3. Velocity-depth functions at OBS site 26 on line 2 (solid line) and site 3 on line 1 (dashed line). Note that, on average, the crust on the Nazca Plate at 17°15′S is slightly thinner and has lower upper crustal velocities than the Nazca Plate crust at 15°55′S.

upper crustal velocities than the crust east of the rise axis at 15°55′S.

PmP and Pn travel times depend not only on crustal thickness but also on the velocity in the lowermost crust and uppermost mantle. An increase of 0.4 km/s in the lowermost crust P-wave velocity yields a crustal thickness ~0.5 km greater than our estimates, but increases the overall root mean square (rms) misfit by ~20 ms. Best fits were obtained on every profile for velocities in the lowermost crust of 7.1 and 7.2 km/s in the Nazca and Pacific plates, respectively. Crustal thickness estimates are less sensitive to variations in the upper mantle P-wave velocity, because our data set consists of more PmP than Pn picks (Table 1), but the overall rms misfit depends on such velocity. Best fits were obtained for an upper mantle velocity of 7.7 to 7.8 km/s along the eastern section of line 1 and 7.9 to 8.1 km/s along the rest of the profiles. Our modeling effectively measures the depth to the Moho considered as a velocity discontinuity. Alternatively, the Moho may represent a transition zone with a velocity gradient from 7.2 to >7.7 km/s, but the lack of turning rays in the lower crust did not allow us to discriminate between these models. However, Bazin *et al.* (*12*) obtained similar crustal thicknesses along lines 2 and 3, using a tomographic inversion that considers the Moho as a transition zone. We do not believe that differences in the nature of the Moho (discontinuity or transition zone) can explain the differences in crustal thickness between lines 1 and 2.

The small along-axis difference in crustal thickness found on the Nazca Plate was unexpected, because line 2 is located flankward of a morphologically inflated part of the EPR where a shallow magma chamber has been mapped (*14*, *15*), whereas line 1 is close to the 15°55′S OSC where the axial magma chamber reflector disappears (*14*). A shallow, inflated ridge axis is often interpreted as reflecting a high magma supply, which results in the production of a thicker crust, whereas near a segment end, magma supply is expected to be lower resulting in thinner crust (*16*, *17*). However, recent results suggest that the relation between morphological indicators of magma supply and crustal structure is not this simple (*18*). Thinner crust has been reported on the flanks of an inflated portion of the EPR at 9°50′N than near the ends of this same segment (*19*), and seismic reflection data from both the northern EPR and Valu Fa ridge reveal wide magma chamber reflectors beneath some OSCs (*20*–*22*). On the EPR from 15° to 17°S, the depth and width of the midcrustal magma sill, often taken as an indicator of magma supply, is poorly correlated with axial morphology (*20*).

Thus, we suspect that the slightly thinner ~0.5 to 1.5 million-year (My)-old crust found east of the EPR on line 2 reflects the temporal variation in segmentation geometry along this section of the EPR (Fig. 1). Over the past 1 My, axial discontinuities have migrated rapidly along this portion of the EPR (*5*). The ~1 My-old crust on line 1 may have been generated away from any axial discontinuity, whereas similarly aged crust on line 2 was formed in an OSC (*5*). Thus, the different crustal thicknesses observed between lines 1 and 2 may reflect a difference in magma supply between the end and center of a ridge segment when this crust was formed ~1 My ago. The presence of an OSC may have also produced lateral variations in the upper crustal velocity structure along line 2 (*12*).

Within our estimated uncertainties, the crustal thickness on the Nazca and Pacific plates along both MELT arrays are similar. Along the primary MELT array, teleseismic body waves show that asymmetric P-wave delays are ~0.6 s greater along line 3 than along line 2 (*23*). Averaged crustal travel times along both profiles, within our error estimates, could generate maximum differences of ~0.08 s. Thus, body-wave delay-time anomalies cannot have a crustal origin and must arise from deeper sources. About 150 km from the ridge axis, the MBA is ~18 mGal greater on the Nazca Plate than on the Pacific Plate (*7*). This asymmetry cannot have a crustal origin, because crustal thicknesses and velocities (and therefore, densities) are similar on both plates; a significant east-west variation in mantle temperature or density must be present.

Table 1. Number of picks for each type of ray, coverage, and rms misfit for the best fit models. The travel time picks were obtained from all the seismic traces that show a visually reasonable signal-to-noise ratio.

Line	Number of picks			Off-axis distance of Pg-ray coverage (km)	rms for Pg (ms)
	Pg	PmP	Pn		
1	1033	1671	276	20–70 and 110–170	26
2	803	798	63	30–170	32
3	1363	1008	136	30–250	28

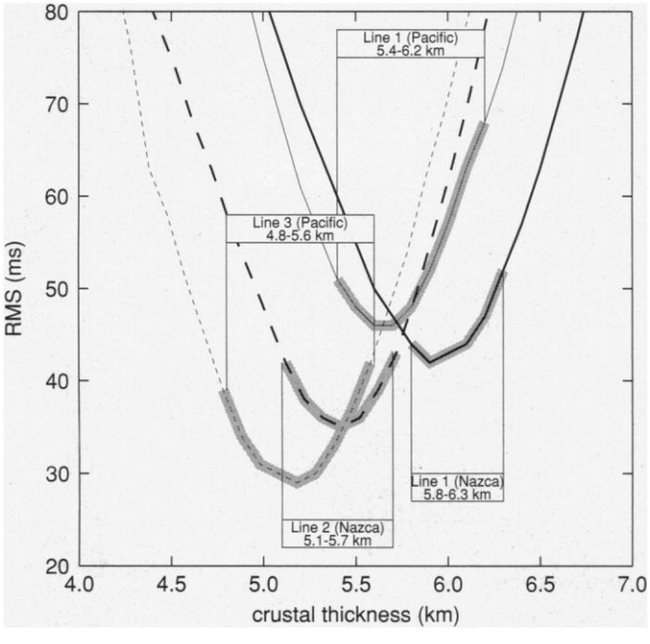

Fig. 4. Rms misfit between observed and predicted PmP and Pn travel times for the eastern and western side of line 1 (thick and thin solid lines, respectively), line 2 (thick dashed line), and line 3 (thin dashed line) plotted as a function of the modeled crustal thickness. The crustal thickness on the eastern side of line 1 is 5.8 to 6.3 km (minimum rms = 42 ms), and on the western side, it is 5.4 to 6.2 km (minimum rms = 46 ms). The crustal thickness along line 2 is 5.1 to 5.7 km (minimum rms = 35 ms), and along line 3 it is 4.8 to 5.6 km (minimum rms = 29 ms). Thus, there is not a resolvable across-axis crustal thickness difference along line 1 or between lines 2 and 3. Crustal thickness uncertainties are shown as gray bands, and they were obtained by selecting those crustal thicknesses for each line that predict residual travel time distributions that have a statistical mean with an absolute value <30 ms. The error bands are not centered about the minimum rms, because the residual mean increases more rapidly for crustal thicknesses less than the optimal value (minimum rms), due to the fact that models with thinner crust do not predict PmP arrivals at all of the offsets observed in the data.

REFERENCES AND NOTES

1. P. Lonsdale, *J. Geophys. Res.* **94**, 12197 (1989).
2. J. M. Sinton, S. M. Smaglik, J. J. Mahoney, K. C. Macdonald, *ibid.* **96**, 6133 (1991).
3. D. S. Scheirer and K. C. Macdonald, *ibid.* **98**, 7871 (1993).

4. L. S. Magde *et al.*, *ibid.* **100**, 3747 (1995).
5. M.-H. Cormier, D. S. Scheirer, K. C. Macdonald, *Mar. Geophys. Res.* **18**, 53 (1996).
6. M. A. Eberle, D. W. Forsyth, E. M. Parmentier, *J. Geophys. Res.*, in press.
7. D. S. Scheirer, D. W. Forsyth, M.-H. Cormier, K. C. Macdonald, *Science* **280**, 1221 (1998).
8. C. DeMets, R. G. Gordon, D. F. Argus, S. Stein, *Geophys. Res. Lett.* **21**, 2191 (1994).
9. The MBA is calculated by removing from the free-air anomaly the gravity effect of the water-crust and crust-mantle boundary topography, assuming a 6-km crustal thickness. The east-west asymmetry of ~18 mGal in the MBA across the EPR at ~15°55′S (*7*) can be explained by an east-west decrease in the mantle density of $\Delta\rho \approx 5$ kg/m^3 within the upper 100 km of the mantle. Assuming that the change in density is caused by thermal expansion, an east-west increment in mantle temperature of $\Delta T \approx 50$°C is required, if the mantle density and the coefficient of thermal expansion are $\rho_m = 3300$ kg/m^3 and $\alpha = 3.1 \times 10^{-5}$ K^{-1}, respectively.
10. J. Willoughby, J. Orcutt, D. Horwitt, *Bull. Seismol. Soc. Am.* **83**, 190 (1993). For a comprehensive overview of the instruments, contact www-mpl.ucsd.edu/obs
11. C. A. Zelt and R. B. Smith, *Geophys. J. Int.* **108**, 16 (1992).
12. S. Bazin *et al.*, *Geophys. Res. Lett.*, in press.
13. Although we find that the best fitting lower crustal velocities are different between the Pacific and Nazca plates, the difference falls within the assigned velocity uncertainty (±0.1 km/s).
14. R. S. Detrick *et al.*, *Science* **259**, 499 (1993).
15. J. G. Mutter *et al.*, *ibid.* **268**, 391 (1995).
16. K. C. Macdonald, J.-C. Sempéré, P. J. Fox, *J. Geophys. Res.* **89**, 6049 (1984).
17. K. C. Macdonald and P. J. Fox, *Earth Planet. Sci. Lett.* **88**, 119 (1988).
18. E. E. E. Hooft, R. S. Detrick, G. M. Kent, *J. Geophys. Res.* **102**, 27319 (1997).
19. G. A. Barth and J. C. Mutter, *ibid.* **101**, 17951 (1996).
20. J. S. Collier and M. C. Sinha, *Nature* **346**, 646 (1990).
21. ———, *J. Geophys. Res.* **97**, 14031 (1992).
22. G. M. Kent, A. J. Harding, J. A. Orcutt, *ibid.* **98**, 13971 (1993).
23. D. R. Toomey, W. S. D. Wilcock, S. C. Solomon, W. C. Hammond, J. A. Orcutt, *Science* **280**, 1224 (1998).
24. Supported by NSF grant OCE 94-03697 to the Woods Hole Oceanographic Institution. J.P.C. was supported by a Ministerio de Educación y Ciencia (Spain)/Fulbright scholarship (FU96-28992999). Woods Hole Oceanographic Institution contribution number 9707.

17 February 1998; accepted 9 April 1998

Shipboard Geophysical Indications of Asymmetry and Melt Production Beneath the East Pacific Rise Near the MELT Experiment

Daniel S. Scheirer,* Donald W. Forsyth, Marie-Hélène Cormier, Ken C. Macdonald

Near the Mantle Electromagnetic and Tomography (MELT) Experiment, seamounts form and off-axis lava flows occur in a zone that extends farther to the west of the East Pacific Rise than to the east, indicating a broad, asymmetric region of melt production. More seamounts, slower subsidence, and less dense mantle on the western flank suggest transport of hotter mantle toward the axis from the west. Variations in axial ridge shape, axial magma chamber continuity, off-axis volcanism, and apparent mantle density indicate that upwelling is probably faster and more melt is produced beneath 17°15′S than beneath 15°55′S. Recent volcanism occurs above mantle with the lowest seismic velocities.

Using multibeam, swath measurements of bathymetry and sea-floor reflectivity, as well as gravity and magnetic field measurements (*1*), we can map the distribution of seamounts and recent lava flows, determine the detailed geometry and history of the plate boundary, and deduce where there are variations in crustal thickness or mantle density. In addition to providing the context for the design of the MELT Experiment, these observations yield indications of the pattern of mantle flow and melt production beneath the axis that complement those from the seismological observations.

The MELT experiment is centered on a linear, 800-km-long section of the East Pacific Rise (EPR) stretching from the Garrett Transform Fault at ~13.5°S to the large overlapping spreading center (OSC) at 20°40′S (Fig. 1). On a finer scale, the plate boundary is disrupted by a series of small, left-stepping, en echelon discontinuities (*2*, *3*) ranging in offset from 1 to ~5 km at the OSC at 15°55′S (Fig. 2). As indicated by subtle variations in sea-floor lava composition, there may be a separate magma source or separate episodes of magma supply for each of the segments separated by these minor discontinuities (*4*). The morphology of the sea floor shows that the OSC locations have changed with time through episodes of rift propagation (*5*, *6*). At 17°S, the Pacific (to the west) and Nazca (to the east) Plates are spreading apart at a full rate of 145 mm/year, a fast rate for present-day mid-ocean ridges. Over the past 5 million years, in this area, rapid rift propagation has transferred seafloor from the Pacific to the Nazca Plates, so that the effective sea-floor spreading rate has been on average 10 to 20% faster to the east than to the west (*2*, *7*, *8*). The combined effects of asymmetric spreading and asymmetric absolute plate motion (Fig. 1) have caused the EPR axis to migrate at about 32 mm/year to the WNW over the hot spot frame of reference in the direction that would tend to keep the spreading center above the regions with the lowest seismic velocities (*9*, *10*).

The axis of the spreading center is along a 5- to 20-km-wide ridge (Fig. 2) that stands 200 to 300 m above the background subsidence of the sea floor. On the basis of the gravity anomalies associated with this feature, it has been suggested that this axial topographic high is isostatically supported by low densities in a narrow conduit filled with partial melt, extending tens of kilometers into the mantle (*11*–*13*). This partial melt zone would correspond to the narrow mantle upwelling center hypothesized in some dynamic models of the spreading process (*14*). However, other models have been suggested for the origin of the axial high that do not require support by buoyant partial melt (*15*).

The axial topographic high is shallower and broader at the latitude of the primary ocean-bottom seismometer (OBS) array than anywhere else in the study area, except for a short, shallow section at about 18°30′S (Figs. 2 and 3). This inflation of the axial ridge is considered to be an indicator of magmatic robustness (*16*). If magma delivery to the crust is not uniform along-axis, inflated areas may lie above centers of upwelling and melt production. Another indication of the overall magma supply, as well as the thermal state of the crust and uppermost mantle, is the mantle Bouguer gravity anomaly (MBA) (*17*). The dominant feature in the MBA is the increase away from the spreading center that is caused by cooling and contraction of the lithosphere with increasing age (Fig. 2B). The lowest values occur where the primary OBS array crosses the ridge, indicating that either the crust is slightly thicker there or the crust and mantle have lower densities. Axial MBA values increase to the north of 17°S and to the south of 18°30′S, reflecting either denser, colder mantle or a decrease in magma supply, leading to thinner crust (the differences could be explained by crust about 400 m thinner near

D. S. Scheirer and D. W. Forsyth, Department of Geological Sciences, Box 1846, Brown University, Providence, RI 02912, USA.
M.-H. Cormier, Lamont-Doherty Earth Observatory of Columbia University, Palisades, NY 10964, USA.
K. C. Macdonald, Department of Geological Sciences, University of California, Santa Barbara, CA 93106, USA.
*To whom correspondence should be addressed. E-mail: scheirer@emma.geo.brown.edu